Optimization of the VERITAS Orbit-Mode Tracking Pattern

Senior Project

Department of Physics

By,

Joshua Allen

May 17, 2012

Supervisor, Dr. Jodi Christensen

Table of Contents

1. Abstract

Gamma-ray Bursts (GRBs) have not been detected at TeV energies. Detection with the Very Energetic Radiation Imaging Telescope Array System (VERITAS) would open a new window into GRB science. In this paper, we optimize an orbit mode tracking method to search for a GRB at a location provided by the FERMI Gamma-ray satellite. Using Matlab we modeled the orbit tracking pattern. Then we found the optimal offset radii and tracking speed for the telescope to form a uniform image exposure. To optimize the pattern, the model accounts for the maximum 1°/s speed of the telescope's tracking motors and the camera's ability to gather light. Using these constraints, we optimized a search pattern to cover varying error circles up to a maximum 3σ error circle ~45° in diameter. As a result of the optimization, VERITAS will have a better chance of observing TeV gamma-rays emitted by a GRB.

2. Introduction

Mankind is obsessed with understanding the unknowns of our observable universe. Physicists currently study Gamma Ray Bursts (GRBs), which are very-high energy (VHE) emissions whose origins are not well understood by the scientific community. Energies from GRBs are high enough to lead some scientists to theorize they could destroy the Earth's ozone layer if one of these events were to occur within our galaxy and it were pointed directly at the Earth. As a result, harmful solar radiation could destroy a large percentage life on Earth similar to the mass extinction of the Ordovician period about 440 million years ago. Currently this explanation is just a theory about the Ordovician extinction, but gives us a gauge of how much energy is released in these bursts [1].

GRBs are known to occur at a frequency of approximately one per day with a uniform sky distribution [2]. More than 40 years after their initial discovery, little is still known about the causes of GRBs with varying theories attempting to create an accurate model of the energy output of the bursts. Currently high energy astrophysicists employ a series of ground and space-based telescopes to detect, analyze, and image gamma ray sources in our surrounding universe including GRBs. Ground-based observatories such as the High Energy Spectroscopic System (HESS), Major Atmospheric Gamma-ray Imaging Cherenkov Telescope (MAGIC), and VERITAS, all currently search for cosmic gamma-ray sources. They are supplemented by space-based observatories such as the Compton Gamma Ray Observatory (CGRO), FERMI Gamma-ray Space Telescope, and Swift Space Telescope, which observe the lower energy photons emitted by gamma-ray sources. Astrophysicists also utilize various radio and optical telescopes to obtain observational data to provide a broad spectrum of these sources. After five years of service, the Swift Gamma Ray Burst Explorer recently detected its 500th GRB on April 13th, 2011. The list of detected GRBs is quite large (~6,000 to date), but they are a challenge to observe because of the short time span over which they occur [3]. Even though thousands of GRBs have been detected, none have been directly observed by a very high-energy gamma ray telescope such as VERITAS, MAGIC, or HESS.

VERITAS observes gamma ray sources to better understand our surrounding universe. The array's uniqueness stems from its design to observe the highest energy particles in the known universe. Currently, VERITAS and HESS are the only telescopes sensitive to 50 TeV gamma-rays [4]. Particles in this energy range from GRBs come from the initial short burst. An afterglow occurs after the initial burst where lower energy particles are emitted over a longer time scale due to the jets slowing down and spreading out laterally [5]. VERITAS works by

collecting UV Cherenkov radiation on the ground and then tracing them back to VHE gamma-rays impacting our atmosphere. To date, VERITAS has not been able to observe these very-high energy gamma rays emanating from a GRB because of the limitations of its observational approach and the uncertainty in location of the source. As the current sit-and-stare approach has not produced results, our goal was to optimize a circular orbit mode approach. The orbit approach has recently been implemented into the tracking software of the array resulting in similar or possibly better sensitivity and more coverage area than previous techniques [6]. In this paper we explore an expanded approach that involves multiple orbits to cover a wider area of the sky, thus increasing the chances of VERITAS observing the highest energy gamma-ray particles in the universe.

3. Gamma-Ray Bursts

3.1 Background

Gamma-Ray Bursts were first detected indirectly in 1967 by the Vela gamma-ray detection satellites which were used to monitor the Earth for illegal Soviet atmospheric nuclear weapons tests. Instead of discovering secret Soviet Nuclear tests, the Vela satellites began to detect high-energy gamma ray photons that could not be associated with the emissions of a nuclear weapon. The source of these detected gamma-ray photons was not understood, until astrophysicists proposed the idea that the gamma-rays could be of a cosmic origin [7]. Since the first observations, GRBs have been an important field of study for high-energy astrophysicists. The source of GRBs has not been confirmed, however, current models link these high energy emissions to relativistic beamed jets produced during a supernova explosion as shown in Figure 1, or from merging black holes and neutron stars.

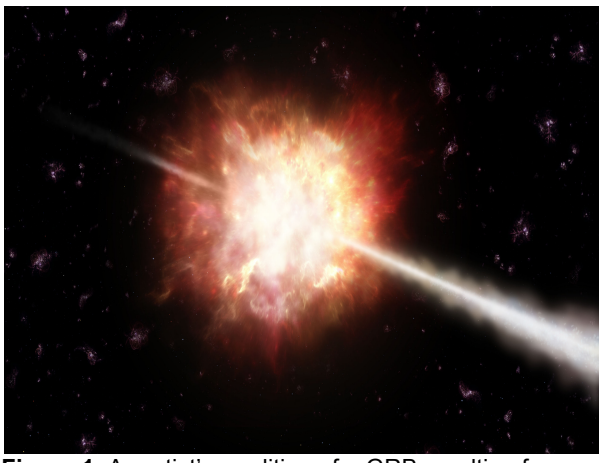

Figure 1. An artist's rendition of a GRB resulting from a supernova. The picture shows two bipolar relativistic jets of high-energy particles [8].

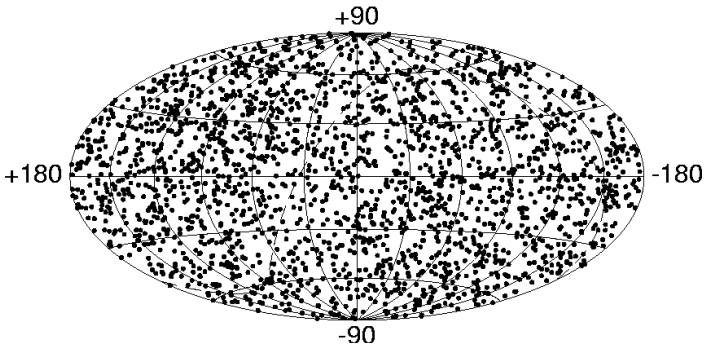

Figure 2. Detected GRB events from the Burst and Transient Source Experiment showing the uniformity of GRB occurrence in our universe [9].

3.2 GRB Source Theory

All three potential causes of GRBs are massive objects collapsing in on themselves, which results in a release of high-energy photons. A popular hypothesis is that supernovae also produce focused beams of intense radiation with the most energetic gamma-ray photon emissions lasting ~100-1000 seconds. GRB emissions along the jets should contain energies from radio to TeV, making them the most energetic accelerators in our universe since the big bang [10]. However, we can only observe these sources if one of the bipolar jets is pointed at the Earth. VERITAS searches for this wave of gamma-ray particles when they interact with our atmosphere. Current models use relativistic beaming to explain the extreme energies observed. Without the jets and relativistic beaming, the emissions would be difficult to explain as a result of single star exploding. Because the extreme energies of these particles cannot be fully explained, other theories have emerged involving the merger of two of the densest objects in our universe. Models have shown that if two neutron stars merged from 45 km apart, each with a mass of 1.5 Suns, the result could produce relativistic-jets and a magnetic field strong enough to become a central engine in a short Gamma Ray Burst [11]. An alternate theory involves the same concept as the neutron star model, but with two black holes merging together producing the same effect. All of these models agree that releasing particles with energies similar to those found in GRBs would require the collapse or merging of highly dense objects.

GRB sources have been detected on a regular basis by satellites such as FERMI, which detected 438 GRBs from June 2008 to March 2010. Their detected locations have been uniformly distributed across the sky, which imply these bursts occur outside of our galaxy [12]. Other observatories, such as the Burst and Transient Source Experiment (BATSE) onboard CGRO, have plotted GRB location data, shown in Figure 2, which leads to similar conclusions.

3.3 Types of GRBs

The analysis of GRB data acquired by gamma ray observatories has led to classification of the bursts into two categories, long and short [13]. The difference between long and short GRBs is defined by the length of time of their initial burst. Short GRBs last about 1-2 seconds, whereas, long GRBs occur over a much lengthier period. Short and long GRBs have similar types of emission spectra in the first few seconds of the burst implying that the two events dissipate the same way initially. However, long GRBs emit high energy particles beyond the initial burst implying that the latter emissions can be attributed to a different type of event with a longer energy emission period [14]. The time profile of short GRBs makes them almost impossible to observe unless the telescope is pointing directly at the source at the instant the event occurs. Long GRBs have a much higher probability of being observed because they continue to emit high-energy particles for a time period long enough for the various gamma-ray observatories to move to the source and begin acquiring data. Even though GRBs occur regularly, they are not well understood and VERITAS observations will study the highest energy gamma-rays, above what the FERMI satellite, its space-based relative, can detect.

4. Hardware and Detector

4.1 VERITAS

The Very Energetic Radiation Imaging Telescope Array System (VERITAS) is a ground-based, gamma-ray telescope system, located at the Whipple Observatory in Arizona. It is

designed to track and gather energy spectra of gamma-ray sources in our observable universe. VERITAS has many science goals associated with its ability to observe high energy gamma rays including: the detection of dark matter through the annihilations of Weakly Interacting Massive Particles (WIMPs), active galactic nuclei observations, blazar discovery, and black hole emission observations [15]. One of the science goals of the telescope is to observe the GeV to TeV energy spectra of Gamma-Ray Bursters. The array includes four, 12-meter diameter Davies-Cotton telescopes [16]. A Davies-Cotton reflector optical system utilizes a large spherical primary mirror with a radius equal to its focal length. The Davies-Cotton design is widely used in ground based gamma-ray observatories because of the large light-collecting surface area. These types of telescopes are designed to have a wide viewing angle and reduce aberrations that effect traditional spherical and parabolic ground based telescopes [17]. By setting up an array of four Cotton-Davies type telescopes, VERITAS is able to utilize the stereoscopic imaging atmospheric Cherenkov technique (IACT).

The array uses four telescopes to increase its overall ability to collect light resulting in a higher sensitivity than a single telescope. Using four telescopes to acquire data, VERITAS is able to create stereoscopic images by overlaying the images from each separate telescope. One VERITAS telescope has 350 equally-sized, highly-reflective, hexagonal mirror facets each with an area of 0.322 m^2 giving the Cotton-Davies reflector a total light collecting area of ~110 m^2. Each one of the hexagonal pieces has three adjustment screws used to align the mirrors to create one large continuous mirror [16].

4.2 Imaging Atmospheric Cherenkov Technique (IACT)

The IACT is a method of detecting very high energy gamma-rays hitting the Earth's atmosphere by observing the resultant ultraviolet photons called Cherenkov radiation. VHE gamma-rays impact molecules in our upper atmosphere beginning a chain of events resulting in the creation of a Cherenkov radiation shower. The incident gamma-ray collides with the nucleus of an air molecule causing it to undergo a positron and electron pair production [18]. These positrons and electrons are extremely energetic due to the energy transfer and travel at speeds faster than the speed of light in air. As a result of all of these highly energetic particles traveling beyond the phase velocity of light, a collimated shower of UV radiation is created in a cone shape towards the ground as shown in Figure 3 [19].

This "cone" of UV radiation travels in the same direction as the incident gamma-ray allowing for the VERITAS to reverse engineer the gamma-ray's direction and energy. VERITAS is able to capture these lower-energy Cherenkov photons to recreate an image of their causal gamma-rays. [18]. Using multiple telescopes employing the Cherenkov imaging technique, VERITAS is able to increase its light sensitivity and it's angular and energy resolution, providing us with stereoscopic image of our GRB source [20].

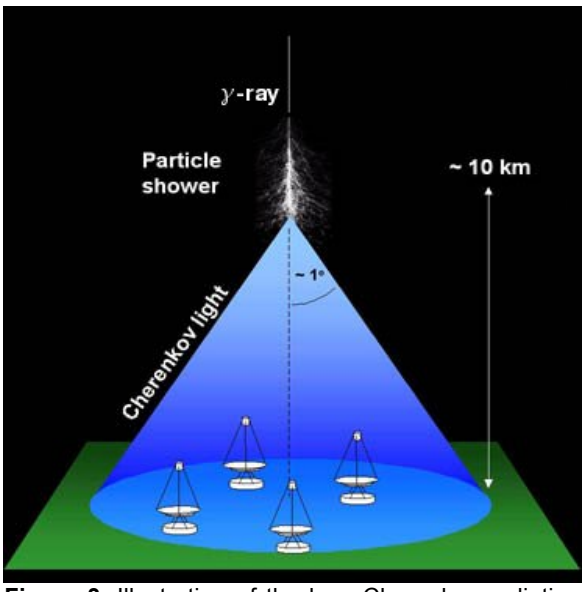

Figure 3. Illustration of the how Cherenkov radiation is observed by VERITAS observes due to cosmic gamma-rays [21].

4.3 VERITAS Imaging System

To capture an image of a gamma-ray source, VERITAS is outfitted with an imaging system that utilizes 499 Photomultiplier tubes (PMTs) as separate pixels to create an image. Each of the PMT is placed with an angular spacing of 0.15° giving the camera a total field-of-view of approximately 3.5° in diameter [16]. The PMTs collect and create a voltage pulse for the Cherenkov UV photons, which is then passed through a discriminator to determine if the source of the photons was indeed from a gamma-ray source. To increase the efficiency of the imaging system and to eliminate ambient light sources, light cones were installed in front of the camera [22]. When the discriminator threshold is reached on three adjacent PMTs, the software digitizes the signal by sending the results into a custom built Flash-ADC (analog to digital conversion) system [20]. VERITAS is able to create an energy spectrum for a gamma-ray source by a backwards energy conversion from the Cherenkov radiation to the high-energy gamma-ray that caused it.

5. VERITAS GRB Tracking

5.1 Locating a GRB Source

To observe GRBs, VERITAS relies on location data provided by the FERMI Gamma-Ray space telescope, which detects and observes gamma-ray sources using its Large Area Telescope (LAT) and Gamma-ray Burst Monitor (GBM) [23]. After detecting gamma-rays from a potential GRB source, FERMI uses a series of algorithms to find the exact location of the source in the sky. This location is then broadcast onto the web along the Gamma-ray Burst Coordination Network (GCN). VERITAS extracts the data from the GCN provided by FERMI to locate potential observable sources [24]. VERITAS is used for follow-up studies at energies higher than FERMI LAT's observable energy range of 300 GeV [23]. As VERITAS performs its follow-up observation, FERMI continually reduces the uncertainty of the source's location as it continues its observation of the source. FERMI broadcasts updates of the source's location over

the GCN providing telescopes like VERITAS progressively more accurate GRB coordinates. [24]. The location algorithms on the FERMI satellite can yield error bars much larger than VERITAS's field-of-view, so VERITAS employs a filter to pursue locations with an error of <7.5° in radius. Because of the large initial uncertainty of the location of the source, VERITAS has to search around the supposed area to gather an image of the source.

5.2 VERITAS Tracking System Hardware

Each telescope is mounted on a tubular steel frame Optical Support Structure (OSS) which utilizes an altitude-over-azimuth positioner system to track and observe gamma-ray source locations provided by the FERMI satellite. The system uses two motors to rotate the telescope into the correct position to observe a source. Each of these motors have a tracking speed limit of 1° per second with a pointing accuracy of <±0.01° [20].

5.3 VERITAS Current Observation Techniques

VERITAS usually observes the source from a point offset 0.5° from the origin in the four cardinal directions as shown in Figure 4a. Typically the array observes for 20 minutes at each of the four points using a "wobble mode" method. Using this method the telescope "sits and stares" at one location offset from the known location to gather photons for a 20 minute period. This method repeats the "sit and stare" routine four times making the maneuver's total observation time around 80 minutes. By offsetting the telescope from the GRB source origin, VERITAS is able to characterize the background more reliably. Although it provides ample time to collect photons to create an image, the wobble-mode approach is limited to a small coverage area over a long period of time [6].

We explored a new "orbit mode" method to increase the efficiency for the GRB search. The orbit-mode approach follows a circular track pattern around the source at a specific radial offset and angular velocity shown in Figure 4b. This method reduces and blurs the background signals from stars due to a stationary observation in the wobble-mode method. Although more tests are needed for verification, initial tests show an overall increase in sensitivity [6].

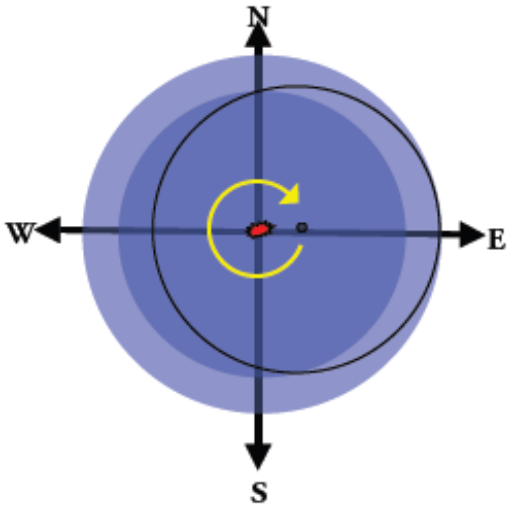

Figure 4a. "Wobble" mode observation approach with 4 cardinal direction offset. The red dot in the center represents the calculated source origin [6].

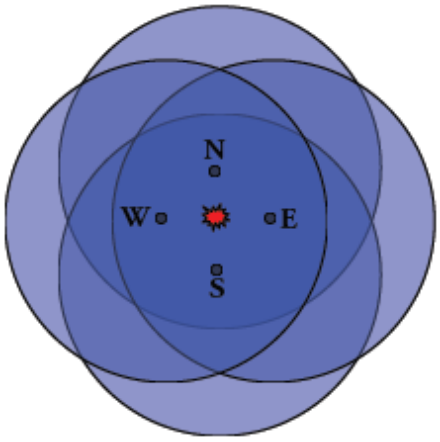

Figure 4b. "Orbit" mode observation with radial offset. The red dot in the center represents the calculated source origin and the green dot represents the center of the telescope at its offset [6].

6. Optimization of Orbit Tracks

The end goal of our analysis was to determine values for the radial offset and tracking speed for a series of concentric tracking circles that provide a uniform exposure of the sky over the entire search area in the minimal amount of time. We expanded our tracking pattern from the initial "one orbit" pattern described in Figure 4b to cover a larger search area. To accomplish this we ran multiple orbits, each more offset from the origin than the last as shown in Figure 5.

6.1 VERITAS's Camera Acceptance

The camera's efficiency of gathering light is referred to as its acceptance. To characterize the camera acceptance we analyzed the camera's ability to collect light as a function of the radial distance from the center of the camera. To get a function for the VERITAS's acceptance, we used raw data from a known gamma-ray source previously profiled by the telescope. The data we used to find our acceptance for VERITAS was from data taken during Nov. 16, 2009 observation of the Crab Nebula [25].

The relative photon collection rate of the camera is shown in Figure 6 plotted as a function of the radial distance in degrees from the center of the telescope. The relative photon collection rate is normalized using the following equation,

$$\text{Relative rate} = \frac{\text{Photon Rate}}{\text{Maximum Photon Rate}} \tag{1}$$

where the relative rate is ratio compared to the maximum collection rate of the telescope during a 20 minute observation.

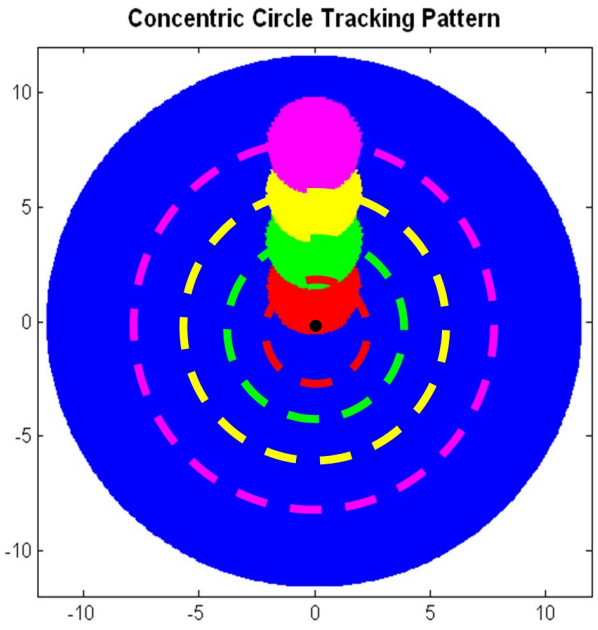

Figure 5. This diagram shows the concentric circle orbit track approach to account for a large location error. The black dot represents the FERMI GRB source location.

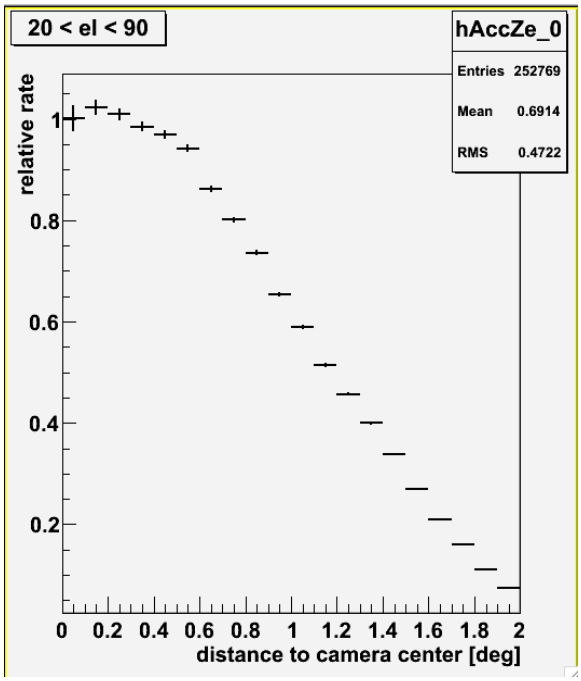

Figure 6. VERITAS camera acceptance plot showing the decreasing light sensitivity away from the center of the camera [25].

The curve in Figure 6 shows VERITAS's relative rate decreasing radially from the center of the telescope with sharp decrease in overall acceptance beyond 0.55°. VERITAS's acceptance decreases to approximately 50% of its maximum at 1.15° radial distance from the center of the telescope and reduces to about 10% at the edge of the telescope. The sharp radial decrease in light collecting ability of the telescope forced us to overlap the tracks for the proposed concentric circle approach to ensure a uniform image exposure. To obtain a function for the radial acceptance we mirrored the data around the origin to get a complete 2-D acceptance profile of VERITAS shown in Figure 7.

In Graphical Analysis, we fit a Gaussian curve to the data which gave us the best RMSE value, which gave us the following equation for the camera's acceptance

$$A(r) = 1.274 \times e^{-(r/1.606)^2} - 0.2313 \qquad (2)$$

where A is the camera's acceptance and r is the radial distance from the center of the telescope in degrees.

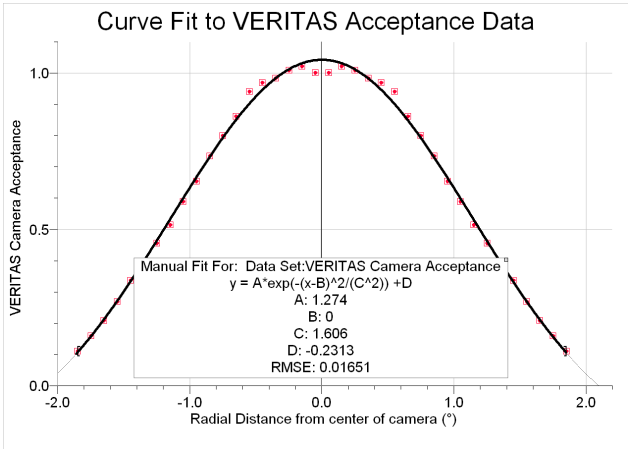

Figure 7. Gaussian Fit to acceptance data. It is mirrored around the center of the camera.

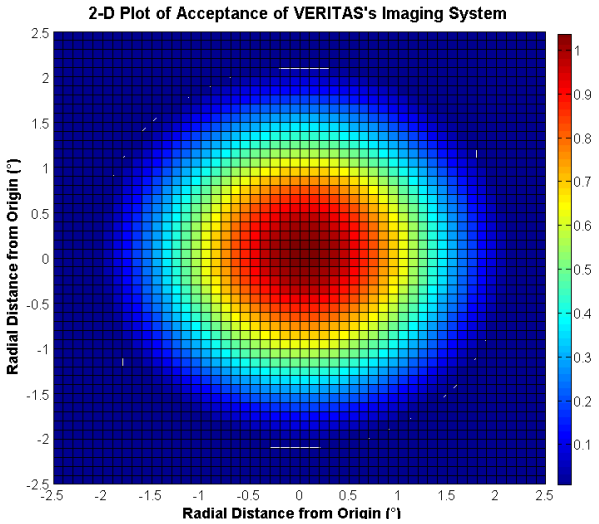

Figure 8. The overall acceptance (light capturing ability) of VERITAS's imaging system.

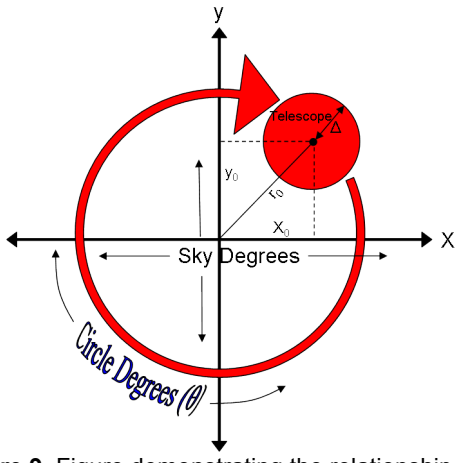

Figure 9. Figure demonstrating the relationship of sky degrees to tracking circle degrees.

6.2 VERITAS Orbit Mode Model

Using the Gaussian fit, we created a 2-D contour plot of VERITAS's acceptance shown in Figure 8. We created a model for a circular tracking orbit to create an acceptance curve for the telescope as it travels in a circular path. Figure 9 illustrates how we parameterized the observation locations in the camera. The location of each point in sky coordinates is given by *x(t)* and *y(t)*.

$$x(t) = (r_0 + \Delta)\cos(\theta(t)) \tag{3}$$

$$y(t) = (r_0 + \Delta)\sin(\theta(t)) \tag{4}$$

$$r_0 = \sqrt{x_0^2 + y_0^2} \tag{5}$$

where r_0 is the radial track offset in sky degrees, Δ is the radial distance in sky degrees from the camera center, and $\theta(t)$ represents the angle in tracking circle degrees at time t around the orbit circle. Notice that Δ can be either positive or negative.

To get θ as a function of the time traveled around the tracking circle we define,

$$\theta(t) = \omega_{cir} \times t \tag{6}$$

where ω_{cir} is the angular velocity in tracking circle degrees per second. To convert the telescope tracking speed in circle coordinates into the angular velocity of the telescope in sky coordinates we used the following conversion,

$$\omega_{cir} = \frac{360° \times \omega_{tel}}{2\pi \times r_0} \tag{7}$$

where ω_{tel} is the angular velocity of the telescope set by the tracking motors in sky degrees per second. The conversion relates the tracking pattern orbit units to the units of the angular velocity of the telescope's tracking motors. This directly correlates the orbit units to units used in sky observations. To get an overall acceptance over a track we integrated the acceptance function around an orbit:

$$\mathrm{A}_{\mathrm{single\,track}} = \int_0^{t_{orb}} A(r(t)) \cdot dt \tag{8}$$

where the time to go around a full orbit is:

$$t_{orb} = \frac{360°}{\omega_{cir}\left(°/_{s}\right)} \quad . \tag{9}$$

A(r) in equation (2) is expressed as a function of time because, $r(t) = \sqrt{x(t)^2 + y(t)^2}$. The algorithm uses the angular velocity of the telescope during the orbit (ω_{cir}) and analyzes the

differences in acceptance and exposure time of the inner part of the orbit (i.e. $r_0 - \Delta$) as compared to the outer part of the orbit (i.e. $r_0 + \Delta$).

The part of the orbit where $r < r_0$ collects slightly more photons because the exposure is longer than when $r > r_0$. The angular velocity, ω_{cir} of the telescope increases with the radial distance from the tracking origin. This reduces the exposure time for points further than r_0, which results in a lower acceptance value. As a result of this radial change of ω_{cir} the final acceptance curve for VERITAS following a circular path is no longer strictly Gaussian, but is weighted towards the inner half of the telescope.

6.3 Varying Track Speed Approach

We optimized the tracking orbit's radial offsets, r_0, and telescope angular velocities, ω_{tel}, to reduce the overall exposure time needed to observe a wide observation area as well as maintain a uniform exposure. We started by optimizing the first orbital track. We positioned the offset the center of the telescope from the origin to prevent overexposure of the center, but still maintain a uniform exposure of the center of the search area. Uniformity of the image exposure for the entire tracking pattern was determined by minimizing the RMSE of the overall acceptance value. To minimize overall tracking orbit time we chose the ω_{tel} of the first track to be the maximum allowable speed of 1°/s. We found that to provide a uniform image exposure in the center of our observation area we could only cover ~3° diameter observation circle shown in Figure 10.

To account for the significant GRB location error from the FERMI satellite, more circular paths were needed to provide a uniform exposure over a wider coverage area. In the model, we added secondary track offsets further from the origin than the first track Because the telescope has to travel a longer distance in the outer tracks we reduced the telescope angular velocities ω_{tel}. By decreasing ω_{tel} of the outer track, we allowed the telescope to increase the exposure time at any given point around the path thus providing us with a more uniform image exposure relative to the first tracking orbit acceptance curve from Figure 10.

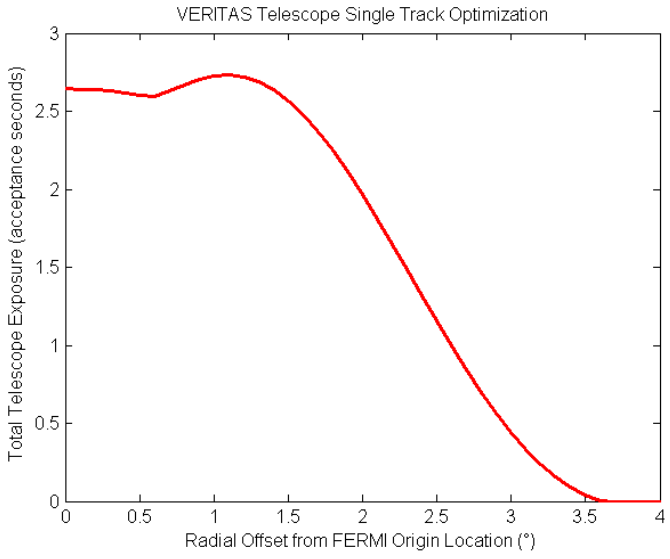

Figure 10. Acceptance curve for a single track orbit with an offset of 1.55° and ω_{tel} of 1°/s.

Figure 11 shows the orbit offsets and telescope tracking speeds optimized for uniform exposure. To get one total acceptance curve (shown as the blue line in Figure 11 and 12), we integrated all the offset acceptance curves in the tracking pattern using the equation,

$$\text{Total Exposure (acceptance} \circ \text{sec)} = \int_{t=0}^{t=\text{time for all tracks}} \sum_{i=1}^{i=\text{total \# of tracks}} A_{\text{single track } i} \bullet \Delta t \quad . \tag{10}$$

To further expand beyond our initial orbit mode approach covering a 1σ (7.5° maximum) FERMI error circle, we added more tracks to the model to cover up to 3σ as shown in Figure 11. Expanding to a 3σ error circle allowed us to optimize an orbit approach with ~100% probability of locating the GRB source within the coverage area.

In Table 1, each row represents an additional track added to the search pattern to widen the search area up to 3σ. By optimizing ω_{tel} and r_0, we see in Table 1 the most uneven exposure difference is 5.33% during a two orbital track approach. Using 11 tracks, we expanded the pattern to cover a search circle up to a radius of 22.79°, which accounts for the entire 3σ error circle of the maximum error accepted by VERITAS of 7.5°.

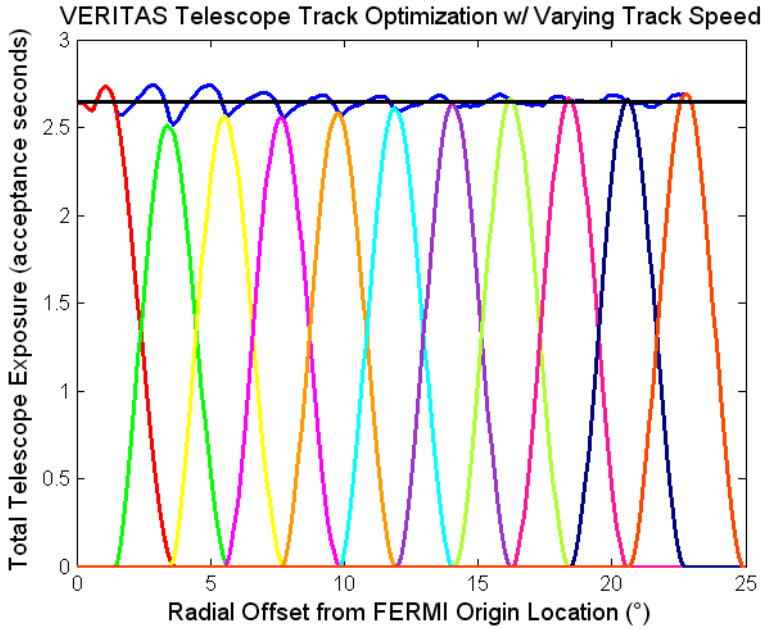

Figure 11. Track offsets and acceptance curves to cover 3σ GRB search area using a varying track speed orbit method. Offset and track speed values are shown in Table 1. Each successive track is indicated by a separate color with the total exposure indicated in blue and the overall average indicated in black.

Track #	Tracking Speed, ω_{tel} (°/s)	Radial Track Offset, r_0 (°)	Average Exposure (acceptance◦sec)	Maximum Total Exposure	% from Avg.	Minimum Total Exposure	% from Avg.
1	1	1.55	2.6524	2.733	3.04%	2.567	-3.22%
2	0.98	3.55	2.6588	2.743	3.17%	2.517	-5.33%
3	0.95	5.6	2.6564	2.743	3.26%	2.517	-5.25%
4	0.95	7.69	2.6528	2.743	3.40%	2.517	-5.12%
5	0.94	9.8	2.6478	2.743	3.60%	2.517	-4.94%
6	0.93	11.93	2.646	2.743	3.67%	2.517	-4.88%
7	0.92	14.08	2.6452	2.743	3.70%	2.517	-4.85%
8	0.91	16.25	2.6452	2.743	3.70%	2.517	-4.85%
9	0.91	18.43	2.6455	2.743	3.69%	2.517	-4.86%
10	0.91	20.6	2.647	2.743	3.63%	2.517	-4.91%
11	0.9	22.79	2.6473	2.743	3.62%	2.517	-4.92%

Table 1. Optimized Track speeds and radial offsets for varying track speed orbit method covering a 3σ error circle.

6.4 Maximum Tracking Speed Approach

Another approach we explored was to cover the area as fast as possible by maximizing the speed of every track regardless of its radial offset. By maximizing the angular velocity, the outer tracking orbits show a reduced overall acceptance because of the longer path distance, which results in less time collecting photons at any given point around the track path. We offset this effect by decreasing the offsets so that the orbits overlap more. For the most uniform exposure over a wide coverage area we optimized the radial offsets of each track for a maximum ω_{tel} of 1°/s.

We expanded our search pattern to cover up to a 3σ search area and optimized the offsets for all of the required tracks shown in Figure 12. We see the acceptance curves overlapping more than they did in the varying speed approach to account for the reduced exposure. Table 2 shows the parameters for the maximum tracking speed approach shown in Figure 12.

From Table 2, we see the maximum difference from the average image exposure is 5.73% for the 4 track maximum tracking speed orbit mode. To optimize the maximum speed approach we had to overlay the tracks more than the vary speed approach. This is a result of the lack of exposure time of the telescope at the outer radii. The data in Table 2 implies the maximum speed approach would have a less uniform image over the same coverage area as the varying speed approach.

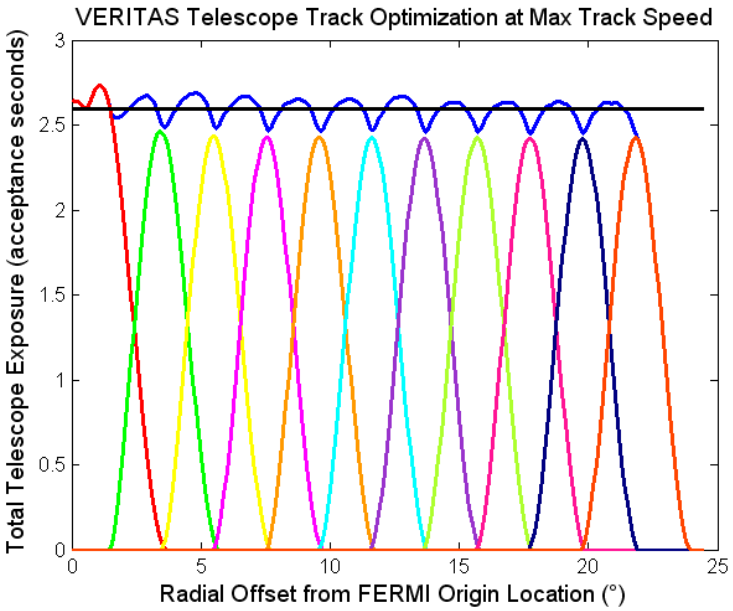

Figure 12. Track offsets and acceptance curves to cover 3σ GRB search area using 1°/s track speed orbit method. The radial offsets for each track are shown in Table 2. Each successive track is indicated by a separate color with the total exposure indicated in blue and the overall average indicated in black.

Track #	Radial Track Offset, r_0 (°)	Average Exposure (acceptance◦sec)	Maximum Total Exposure	% from Avg.	Minimum Total Exposure	% from Avg.
1	1.55	2.6524	2.733	3.04%	2.574	-2.96%
2	3.57	2.6281	2.733	3.99%	2.487	-5.37%
3	5.58	2.6199	2.733	4.32%	2.476	-5.49%
4	7.6	2.6147	2.733	4.52%	2.465	-5.73%
5	9.63	2.6077	2.733	4.81%	2.464	-5.51%
6	11.66	2.6044	2.733	4.94%	2.464	-5.39%
7	13.68	2.6038	2.733	4.96%	2.458	-5.60%
8	15.72	2.5995	2.733	5.14%	2.455	-5.56%
9	17.76	2.597	2.733	5.24%	2.453	-5.54%
10	19.8	2.5941	2.733	5.35%	2.448	-5.63%
11	21.84	2.5925	2.733	5.42%	2.448	-5.57%

Table 2. Radial offsets optimized for maximum tracking speed of 1°/s to cover a 3σ error circle.

7. Results

To account for the maximum coverage area due to a FERMI error of 7.5°, we included additional tracking circles as shown in Figure 5, whose acceptance curves were integrated to get an overall acceptance curve for the total maneuver. We concluded that 11 tracks were necessary to cover a 3σ error circle. We optimized the first track's radial offset to provide a uniform exposure at the maximum tracking rate of 1°/s. Each successive tracking orbit's offset and speed was optimized to provide a uniform exposure that extended far enough to cover the maximum error in source location from FERMI.

We evaluated the efficiency of our search patterns by comparing them to the acceptance curve shown in Figure 6, which is data taken from a 20 minute sit-and-stare run. Tables 3 and 4 show how the acceptances of the varying and maximum track speed methods compare to the sit-and-stare method. Tables 3 and 4 show the total time each orbit method would take to be completed once. The tables also show the probability of the source's location within the search circle for each additional track based on the VERITAS's maximum allowable radial uncertainty of a FERMI GRB location. We calculated the likelihood of the GRB source being located within a uniformly exposed search circle of radius r_0 created by our tracking pattern. The source detection probabilities in Tables 3 and 4 are based off a normal distribution probability with a 1σ-value of 7.5° radius. The acceptance of each method is compared to the 20 minute sit-and-stare run by evaluating what ratio of photons VERITAS could acquire if it repeated the search pattern for 20 minutes. The last column in Tables 3 and 4 show the number of 20 minute runs each pattern would require to equal the same overall acceptance of the 20 minute sit-and-stare run. Because every additional track covers more search area in the same amount of time it has less overall acceptance. Therefore, repeating runs is required to reach the equivalent acceptance as the 20 minute sit-and-stare run. Each row shows how the acceptance, time, and coverage area change with every additional track.

We see in Tables 3 and 4 that as additional tracks are added to both methods the overall pattern time is increased as the area covered by the telescope increases. As a result of a larger area covered, we see an increase in the total coverage area and detection probability, while sacrificing overall acceptance. Using the orbit tracking methods we sacrifice overall exposure of the image to cover a large search area in a minimal amount of time. In comparing Tables 3 and 4, we see in general the maximum speed method takes less time than the varying speed method because it has a higher tracking speed for the outer tracks. To create a uniform exposure the maximum speed method has smaller radial offsets than the varying speed method forcing the acceptance curves of the additional tracks to overlap more. Overlapping these curves builds up the acceptance in areas where the increased speed causes severe drops in overall exposure time. Intuitively, the larger the coverage area of the pattern, the longer it takes and the less photons the telescope is able to collect at any given point in the search area.

# of Tracks	Total Time for All Tracks (s)	σ-Value of Outer Track Offset	Total Coverage Area (degrees^2)	GRB Detection Probability	Normalized Acceptance for 20 min run (acceptance)	# of Iterations for Equivalent Exposure
1	9.7389	0.21	7.55	16.63%	0.2714	4
2	32.4994	0.47	39.59	36.16%	0.0813	12
3	69.5371	0.75	98.52	54.67%	0.0380	26
4	120.3979	1.03	185.78	69.70%	0.0220	46
5	185.9035	1.31	301.72	80.98%	0.0142	70
6	266.5039	1.59	447.13	88.82%	0.0099	101
7	362.6639	1.88	622.81	93.99%	0.0073	137
8	474.8637	2.17	829.58	97.00%	0.0056	180
9	602.1154	2.46	1067.09	98.61%	0.0044	228
10	744.3502	2.75	1333.17	99.40%	0.0036	282
11	903.4544	3.04	1631.69	99.88%	0.0029	342

Table 3. Data for varying track speed orbit mode method for tracks covering up to 3σ error circle.

# of Tracks	Total Time for All Tracks (s)	σ-Value of Outer Track Offset	Total Coverage Area (degrees^2)	GRB Detection Probability	Normalized Acceptance for 20 min run (acceptance)	# of Iterations for Equivalent Exposure
1	9.7389	0.21	7.55	16.63%	0.2714	4
2	32.1699	0.48	40.04	36.88%	0.0822	12
3	67.2301	0.74	97.82	54.07%	0.0393	25
4	114.9823	1.01	181.46	68.75%	0.0230	44
5	175.4894	1.28	291.34	79.95%	0.0151	66
6	248.7513	1.55	427.12	87.89%	0.0106	94
7	334.7053	1.82	587.93	93.12%	0.0079	127
8	433.477	2.10	776.35	96.43%	0.0061	164
9	545.0664	2.37	990.91	98.22%	0.0048	206
10	669.4735	2.64	1231.63	99.17%	0.0039	253
11	806.6983	2.91	1498.49	99.64%	0.0033	305

Table 4. Data for maximum track speed orbit mode method for tracks covering up to 3σ error circle.

8. Conclusion

We designed a tracking pattern for VERITAS enabling it to observe a large field-of-view. The results of implementing this tracking strategy should provide an increased chance of GRB detection and observation. By implementing the concentric circle tracking pattern, we optimized VERITAS's GRB observation approach. We utilized the maximum tracking speed of the telescope in an orbit mode and the acceptance of VERITAS in our optimization approach. We increased the overall coverage area significantly from the "wobble" mode approach using our tracking pattern.

The current setup of our model is designed to cover the FERMI location and up to the 3σ error circle for the maximum allowable 7.5° radial location error around the calculated location. . Depending on the parameters of the search, VERITAS scientists can evaluate whether it is necessary to search quickly using the maximum speed method or create a more uniform image using the varying track speed method. Depending on the uncertainty of the FERMI source location, the decision can also be made to utilize only a portion of the 11 tracks to cover the necessary search area. During the course of the observation, FERMI updates and more accurately measures the location data to which VERITAS can adjust its tracking pattern accordingly.

The tracking pattern optimization algorithm we used in this analysis can be adjusted to account for any new acceptance curve allowing it to be applied to multiple telescopes or reapplied to an upgraded VERITAS. Currently, the VERITAS group is looking to increase the capabilities of the telescope by installing faster tracking motors, which would increase the tracking speed of the telescope, thus allowing it to cover a larger area in a smaller amount of time. Faster tracking motors would also reduce the time the telescope takes to move into its observation position once a location is found by FERMI. This search method can be applied to any type of telescope that requires searching a large field-of-view such as surveying the galactic plane.

9. References

[1] Melott, A.L., B.S. Lieberman, C.M. Laird, L.D. Martin, M.V. Medvedev, B.C. Thomas, J.K. Cannizzo, N. Gehrels, and C.H. Jackman. "Did a Gamma-ray Burst Initiate the Late Ordovician Mass Extinction?" *International Journal of Astrobiology* 3.1 (1999): 55-61. Print.

[2] "SWIFT Satellite to Catch the Most Powerful Flashes of Light Known in the Universe." *Imagine The Universe! Home Page*. High Energy Astrophysics Science Archive Research Center, 07 Nov. 2007. Web. 6 June 2011. <http://imagine.gsfc.nasa.gov/docs/features/news/26oct99.html>.

[3] Reddy, Francis. "NASA - NASA's Swift Catches 500th Gamma-ray Burst." *NASA - Home*. NASA Goddard Space Flight Center, 19 Apr. 2010. Web. 2 June 2011. <http://www.nasa.gov/mission_pages/swift/bursts/500th.html>.

[4] "VERITAS: Very Energetic Radiation Telescope Array System." *Welcome to VERITAS!* The VERITAS Collaboration, 2011. Web. 22 May 2011. <http://veritas.sao.arizona.edu/>.

[5] Sari, Re'em, Piran Tsvi, and Jules Halpern. "Jets in GRBs." *Astrophysical Journal.* 519: L17, 1999. Print.

[6] Finnegan, G. *Orbit Mode Observation Technique Developed for VERITAS. 2011.* Poster

[7] Klebesadel R.W., Strong I.B., and Olson R.A. (1973). "Observations of Gamma-Ray Bursts of Cosmic Origin". *Astrophysical Journal Letters* 182: L85.

[8] McDade, Liam. "2012 - Are We All Going to Die?" Sacramento City College. Web. 22 June 2011. <http://scc.losrios.edu/~sah/physics/2012.htm>.

[9] Fishman, G. J. "Observed Properties of Gamma-ray Bursts." *Astronomy and Astrophysics Supplement Series* 138.3 (1999): 395-98. Print.

[10] P. Mészáros. “Gamma-Ray Bursts: Accumulating Afterglow Implications, Progenitor Clues, and Prospects.” *Science*. 5 January 2001: 291 (5501), 79-84.

[11] Rezzolla, L., et. al. "The Missing Link: Merging Neutron Stars Naturally Produce Jet-like Structures and Can Power Short Gamma-Ray Bursts." *Astrophysical Journal* 732 (2011): L6. Print.

[12] Nava, L., G. Ghirlanda, G. Ghisellini, and A. Celotti. "Spectral Properties of 438 GRBs Detected by Fermi/GBM." *SAO/NASA ADS: ADS Home Page*. Astronomy & Astrophysics, 4 Feb. 2011. Web. 11 May 2011. <http://adsabs.harvard.edu/abs/2010arXiv1012.2863N>.

[13] Kouveliotou, Chryssa. et al., "Identification of Two Classes of Gamma-ray Bursts." *Astrophysical Journal* 413.2 (1993): L101-104. Print.

[14] Ghirlanda, G., L. Nava, and G. Ghisellini. "Gamma Ray Bursts: Short vs. Long." *Advances in Space Research* 47.8 (2010): 1332-336. Print.

[15] "VERITAS Science." *VERITAS Education*. The VERITAS Collaboration, 2007. Web. 6 June 2011. <http://veritas.adlerplanetarium.org/science/>

[16] Holder, J., R. Atkins, H. Badran, G. Blaylock, S. Bradbury, J. Buckley, K. Byrum, D. Carterlewis, O. Celik, and Y. Chow. "*The First VERITAS Telescope*." Astroparticle Physics 25.6 (2006): 391-401. Print.

[17] Vassiliev, V., S. Fegan, and P. Brousseau. "Wide Field Aplanatic Two-mirror Telescopes for Ground-based γ-ray Astronomy." *Astroparticle Physics* 28.1 (2007): 10-27. Print

[18] "Air Cerenkov Detectors." *Imagine The Universe! Home Page*. High Energy Astrophysics Science Archive Research Center, 31 Mar. 2011. Web. 5 June 2011. <http://imagine.gsfc.nasa.gov/docs/science/how_l2/cerenkov.html>.

[19] "The VERITAS Project." *VERITAS Education*. 2007. Web. 9 June 2011. <http://veritas.adlerplanetarium.org/project/>.
[20] Holder, J. "VERITAS: Status and Performance." *VERITAS Collaboration*. Proc. of Science with New Generation of High Energy Gamma-ray Experiments. 2006. Print.
[21] "Ground Based Gamma Ray Astronomy." Very High Energy Gamma Ray Group, Department of Physics, University of Durham. Web. 20 May 2011. <http://www.dur.ac.uk/~dph0www4/ground.php>.
[22] Maier, G., et. al. "VERITAS: Status and Latest Results." Proc. of 30th International Cosmic Ray Conference, Merida, Mexico. 2007. Print.
[23] "NASA - Fermi Spacecraft and Instruments." *NASA - Home*. 28 Aug. 2008. Web. 5 June 2011. <http://www.nasa.gov/mission_pages/GLAST/spacecraft/index.html>.
[24] "GCN/Fermi GRB and Transient Notices." NASA Goddard Space Flight Center, 7 June 2011. Web. 9 June 2011. <http://gcn.gsfc.nasa.gov/fermi.html>.
[25]<http://www.hep.physics.mcgill.ca/people/maierg/EVNDISP/radialAcceptances/V5_2009_2010/acceptance-d20091116-N3-7SW-005CU-Moderate.root>